J. Meas. Sci. Instrum., 2024, 15(1): 43-53.
DOI: 10.62756/jmsi.1674-8042.2024005
http://jmsi.publish.founderss.cn/
jmsi@nuc.edu.cn

A recognition method of valve plate wear states of piston pump based on optimized VMD-CWT-CNN

LYU Shangjie*, GU Lichen, GENG Baolong

School of Mechatronic Engineering, Xi'an University of Architecture and Technology, Xi'an 710055, China

***Corresponding author:** LYU Shangjie (1002168781@qq.com)

Received: March 11, 2023 **Revised:** April 16, 2023 **Accepted:** April 19, 2023

Abstract: It is difficult to fully mine the information from that one-dimensional vibration signal that expresses the state characteristics and then early recognize the wear of the valve plate of a piston pump. In view of the excellent image processing capabilities of the convolutional neural networks (CNN), we proposed an optimized VMD-CWT-CNN model to solve the above-mentioned problem. Firstly, continuous wavelet transform (CWT) was used to preprocess the signal to obtain a two-dimensional time-frequency diagram of the signal, which iwasused as one input of the CNN model to convert the state recognition problem into a CNN image recognition problem. Secondly, after optimizing variational mode decomposition (VMD) parameters based on correlation coefficient, the vibration signal was preprocessed by using the optimized VMD, and then based on the principle of maximizing the correlation coefficient and the kurtosis value, three groups of Intrinsic mode function (IMF) with fault characteristics were selected and reorganized into a three-channel one-dimensional signal as another input of the CNN model. Finally, in the CNN model, two paths were converged, and the results of the recognition and classification of the valve plate wear states of the piston pump were obtained. In the experiment, the proposed method we first use the optimized VMD and the CWT to preprocess the vibration signal, respectively, and then combined with the CNN to classify the wear states of valve plates. Experimental results show the recognition effect of the proposed method on the three states of valve plate wear is significantly better than that of the single-input CNN model, the typical deep learning method and the machine learning classifier. The optimized VMD-CWT-CNN method can more accurately recognize the valve plate wear states of the piston pump.

Key words: piston pump valve plate wear; vibration signal; convolutional neural network (CNN); variational mode decomposition (VMD); continuous wavelet transform (CWT)

0 Introduction

Hydraulic systems have been widely used in industrial fields such as transportation, chemical metallurgy and construction machinery. As the energy supply element of a hydraulic system, piston pump has an irreplaceable function[1]. Its working state reflects whether the entire system is operating normally[2]. Due to relatively harsh working environments such as heavy load and frequent impact, the key coupling interface of piston pump is prone to degradation, resulting in a decrease in the reliability and even a failure[3]. The valve plate is the key component distributing high and low pressure oil paths of the piston pump. Due to its structural characteristics, it is unavoidable for the cylinder valve plate pair to be worn during operation. Therefore, timely state recognition of the valve plate of piston pump is of great significance to improve the reliability of the piston pump.

At present, state recognition is mainly realized by detecting the characteristic changes of various signals in different operating states of the system[4]. If valve plate is worn, it will affect the normal operation of the entire piston pump, and one of the manifestations is the abnormal vibration of the pump body. By analysis of the vibration signals of piston pump, scholars have proposed different diagnosis and classification methods for the wear states of valve plates.

By using continuous wavelet transform (CWT) to process the signal, time-frequency distribution diagram that accurately characterizes fault characteristics can be obtained[5]. Hong et al.[6] proposed a draft tube vortex state recognition method based on CWT and convolutional neural network (CNN), which can realize automatic extraction of time-frequency map texture features, avoid manual recognition and simplify feature preprocessing procedure, so as to quickly and accurately recognize the

state of draft tube vortex zone. Variational mode decomposition (VMD) is also an effective method of extracting signal features. Wu et al.[7] and Zhou et al.[8] used VMD to process vibration signals and realized fault diagnosis of gearbox. Wu et al. combined VMD with dispersive entropy and proposed a new method of fault feature extraction. Zhou et al. used the clear signal-to-noise resolution ability of singular value decomposition to optimize the number of VMD components and proposed an improved VMD method for unbalance fault feature extraction of wind turbine gearbox. Feng et al. [9] proposed an improved VMD fault feature extraction method aiming at the problem that random noise, end effects and false components may affect the decomposition accuracy of VMD. Although the signal processed by VMD and CWT have more prominent features than the original signal, its components are still very complex and difficult to be recognized. Only by selecting an appropriate neural network or classifier, the advantages of VMD and CWT can be used effectively for state recognition and failure diagnosis. Both VMD and CWT can extract signal features, but the method of extracting signal features for state recognition and fault diagnosis is easily affected by the environment and relies excessively on expert experience, which is not conducive to the popularization and application of related technologies.

In recent years, with the development of artificial intelligence, CNN has been gradually applied to state recognition and fault diagnosis. It also has achieved some good results[10]. Zhang et al.[11] used a one-dimensional CNN to establish a bearing fault diagnosis model, which can adapt to different working conditions and environmental noises. Wu et al.[12] used a one-dimensional CNN for the fault diagnosis of fixed-axis gearboxes and planetary gearboxes. There have studies on fault diagnosis using two-dimensional images as input. Monteiro et al.[13] used Fourier transform to process gearbox data to obtain the spectrogram, then input it into CNN for fault diagnosis of gear tooth fractures. At present, most of CNN fault diagnosis methods for vibration signals use single-input model, and the input mostly is one-dimensional time series signals. There are not many studies on the application of dual or even multi-path CNNs in fault diagnosis and state recognition. Simonyan et al.[14] first proposed a two-stream network in 2014 to classify video actions. One input of the network is continuous optical flow information, and the other input is a simple series of frames. The training results are combined in the fully connected layer, and the results prove that the training effect of this method is significantly better than that of other single-input models.

In this study, taking the vibration signal as the processing object, we proposed a method of recognizing the wear states of the valve plate of piston pump based on optimized VMD-CWT-CNN. Firstly, the original vibration signal was processed by optimized VMD to obtain the multi-channel one-dimensional signal composed of multiple components. Then, the two-dimensional time-frequency diagram of the original signal was obtained by CWT method. After that, the multi-channel one-dimensional signal and two-dimensional time-frequency graphs obtained by preprocessing were input into the model for training. Finally, the results of diagnosis and classification were obtained.

1 Optimized VMD-CWT-CNN

1.1 CWT

Wavelet transform uses a window that changes with frequency, which is more suitable for processing the signals with transient mutations. CWT is one of wavelet transforms and here was used for signal processing. Its mathematical definition is given as

$$T_{\mathrm{CW},t-f}(a,b)=\left[f(t),\psi_{a,b}(t)\right]=\frac{1}{\sqrt{a}}\int f(t)\psi^{*}\left(\frac{t-b}{a}\right)\mathrm{d}t, \tag{1}$$

where $T_{\mathrm{CW},t-f}(a,b)$ is the wavelet transform time-frequency coefficient matrix; $\psi_{a,b}(t)$ is the wavelet basis function; a is the scale parameter; and b is the position parameter. The scale parameter a represents the expansion and contraction related to the frequency. When its value is large, it is suitable for extracting low-frequency features in the signal, otherwise it is suitable for extracting high-frequency features in the signal. The position parameter b plays the role of translation. From the time domain analysis point of view, CWT maps each transient component of the signal to the position on the time domain plane exactly corresponding to the frequency and time of occurrence of the component.

The coefficient matrix $T_{\mathrm{CW},t-f}(a,b)$ describes the similarity between the signal and the wavelet basis function. The larger the coefficient is, the more similar the detail part of the signal is to the wavelet basis function. Commonly-used wavelet basis functions include Haar wavelet, Coiflets wavelet, Morlet wavelet and complex-Morlet wavelet[15]. In our work, complex-Morlet wavelet was adopted as the wavelet basis function owing to its better adaptive ability.

1.2 Optimized VMD

1.2.1 VMD

VMD is a variable scale signal processing method

proposed by Konstantin Dragomiretskiy in 2014[16]. Its essence is to decompose the signal into a series of IMFs, and each IMF is considered to be an amplitude modulation-frequency modulation signal and is distributed within a limited bandwidth of the center frequency. Therefore, estimating the bandwidths of all IMFs is the main purpose of the VMD. The processing steps of VMD are as follows.

1) The analytical signal of the original signal is calculated by Hilbert transform, and then the frequency spectrum of the signal is modulated to the corresponding base band.

$$H(t)=\left[\left(\delta(t)+\frac{\mathrm{j}}{\pi t}\right)u_k(t)\right]\mathrm{e}^{-\mathrm{j}\omega_k t}. \tag{2}$$

2) The norm of the gradient square L^2 of the demodulated signal is calculated and the constrained variational model is expressed as

$$\min_{\{u_k\},\{\omega_k\}}\left\{\sum_{k=1}^{K}\left\|\partial_t\left[\left(\delta(t)+\frac{\mathrm{j}}{\pi t}\right)u_k(t)\right]\mathrm{e}^{-\mathrm{j}w_k t}\right\|_2^2\right\}. \tag{3}$$

3) The constraint model of Eq. (3) is transformed into a non-constraint model by an augmented Lagrangian function, which is expressed as

$$\begin{aligned}&L\left(\{u_k\},\{\omega_k\},\lambda\right)=\\&\alpha\sum_k\left\|\partial_t\left[\left(\delta(t)+\frac{\mathrm{j}}{\pi t}\right)u_k(t)\right]\mathrm{e}^{-\mathrm{j}\omega_k t}\right\|_2^2+\\&\left\|f(t)-\sum_k u_k(t)\right\|_2^2+\left\langle\lambda_{(t)},f(t)-\sum_k u_k(t)\right\rangle.\end{aligned} \tag{4}$$

4) Using the alternating direction multiplier algorithm to solve Eq. (4), we can get the eigenmode function and its corresponding center frequency as

$$\hat{u}_k^{n+1}(\omega)=\frac{\hat{f}(\omega)-\sum_{i=1,i\neq k}^{K}\hat{u}_i(\omega)+\frac{\hat{\lambda}(\omega)}{2}}{1+2\alpha\left(\omega-\omega_k\right)^2}, \tag{5}$$

$$\omega_k^{n+1}=\frac{\int_0^\infty\omega\left|\hat{u}_k(\omega)\right|^2\mathrm{d}\omega}{\int_0^\infty\left|\hat{u}_k(\omega)\right|^2\mathrm{d}\omega}. \tag{6}$$

5) The Lagrangian multiplier are continuously updated by

$$\hat{\lambda}^{n+1}(\omega)=\hat{\lambda}^n(\omega)+\tau\left(\hat{x}(\omega)-\sum_k\hat{u}_k^{n+1}(\omega)\right). \tag{7}$$

6) For any convergent residual term $\varepsilon>0$, the loop is terminated if satisfies

$$\sum_{k=1}^{K}\left(\frac{\left\|u_k^{n+1}-u_k^n\right\|_2^2}{\left\|u_k^n\right\|_2^2}\right)<\varepsilon. \tag{8}$$

1.2.2 Parameter optimization

The parameter K represents the number of decomposition layers. If K is large, frequency aliasing may occur. If K is small, signal information may be missed. Here, the method of determining the number of modes based on correlation coefficient[17] was used. Under the premise that the maximum center frequency appears in the component, the correlation coefficient between the IMFs is calculated to determine whether there was frequency aliasing between the IMFs, so as to determine the number of IMFs. The correlation coefficient of signal $x(n)$ and signal $y(n)$ is defined as

$$\gamma_{xy}=\sum_{n=0}^{\infty}x(n)y(n)/\sqrt{\sum_{n=0}^{\infty}x^2(n)y^2(n)}. \tag{9}$$

After K is determined by the correlation coefficient, three effective IMFs are further determined based on the maximum signal correlation coefficient and kurtosis value. Kurtosis is a dimensionless parameter, which is only related to the shock signal. It is very sensitive to pulse shock while has nothing to do with the detected piston pump speed, type and load condition. When the piston pump is running without failure, due to the influence of various uncertain factors, the amplitude distribution of the vibration signal is close to the normal distribution. With the intervention of the fault, the probability density of the vibration signal amplitude increases. The distribution of the signal amplitude deviates from the normal distribution. The normal curve appears skewed or scattered and the kurtosis value also increases. That is, the larger the kurtosis value, the more fault characteristic information it contains. The discretization equation of kurtosis is expressed as

$$\beta=\frac{1}{N}\sum_{t=1}^{N}\left(\frac{x_t-\bar{x}}{\delta}\right)^4, \tag{10}$$

where x_t is the signal value; $\bar{x}$ is the mean value of the signal; N is the sampling length; and δ is the standard deviation.

1.3 CNN

CNN is a feedforward neural network that includes the convolution calculations and has a deep structure. Owing to its powerful representation learning ability, CNN is widely used in the fields of image recognition, target detection and machine vision. Its structure is usually composed of input layer, convolutional layer, pooling layer and fully connected layer. In addition, we also used Dropout layer, Flatten layer and Concatenate operations. The classic architecture of CNN is shown in Fig.1.

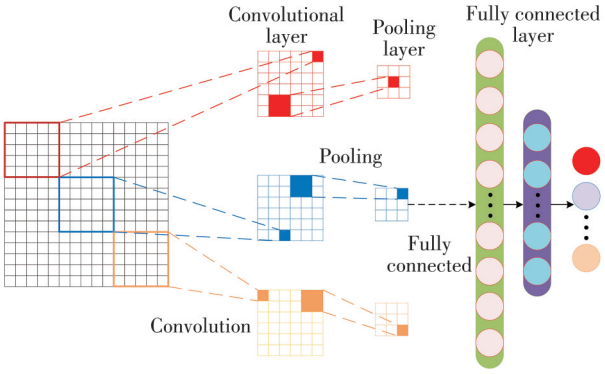

Fig. 1 Classic architecture diagram of CNN

The input layer can recombine the collected signals and send them to the model.

The convolutional layer is used for feature extraction, and the mathematical expression of its operation is

$$z^{(l)} = w^{(l)} \otimes a^{(l-1)} + b^{(l)}, \tag{11}$$

where $z^{(l)}$ is the output of layer l; filter $w^{(l)}$ is the learnable weight vector; $a^{(l-1)}$ is the output of layer $l-1$; and $b^{(l)} \in \mathbb{R}$ is the learnable bias.

The pooling layer is generally connected behind the convolutional layer to reduce the size of the model so as to increase the calculation speed and improve the robustness of the extracted features. The pooling operations are generally divided into three types: Max Pooling, Average Pooling and Global Average Pooling. This study used Max Pooling and Global Average Pooling, and the mathematical expression of the Max Pooling operation is

$$Y_{m,n}^{d} = \max_{i \in \mathbb{R}_{m,n}^{d}} x_i, \tag{12}$$

where x_i is the activation value of each neuron in area $\mathbb{R}_k^d$. In addition, the main purpose of using Global Average Pooling here is to reduce the number of parameters and computational complexity.

The salient feature of the fully connected layer is that all neurons between the layers are connected to each other, which means all the features are connected and then the output value are sent to the classifier.

During the training, the Dropout layer will set thresholds and then compare them with the weights of some hidden layer nodes to make specific weights not work, that is, these weights will be discarded in this layer, which not only speeds up calculations, but also prevents overfitting.

The Flatten layer is used to flatten the input, that is, to make the multi-dimensional input one-dimensional. It is commonly used in the transition from the convolutional layer to the fully connected layer, without any change in batch size.

Concatenate operation is a very important operation in the design of CNN structure. It is often used to fuse features extracted from multiple convolutional feature extraction frameworks or to fuse information from the output layer. In our model, it is used to merge the one-dimensional path and the two-dimensional path.

2 Proposed VMD-CWT-CNN model

The optimized VMD-CWT-CNN model is composed of two paths corresponding to two inputs: one input is the two-dimensional time-frequency diagram processed by CWT, and the other input is the three-channel one-dimensional signal obtained by recombining the one-dimensional signal processed by optimized VMD. The model framework is shown in Fig.2.

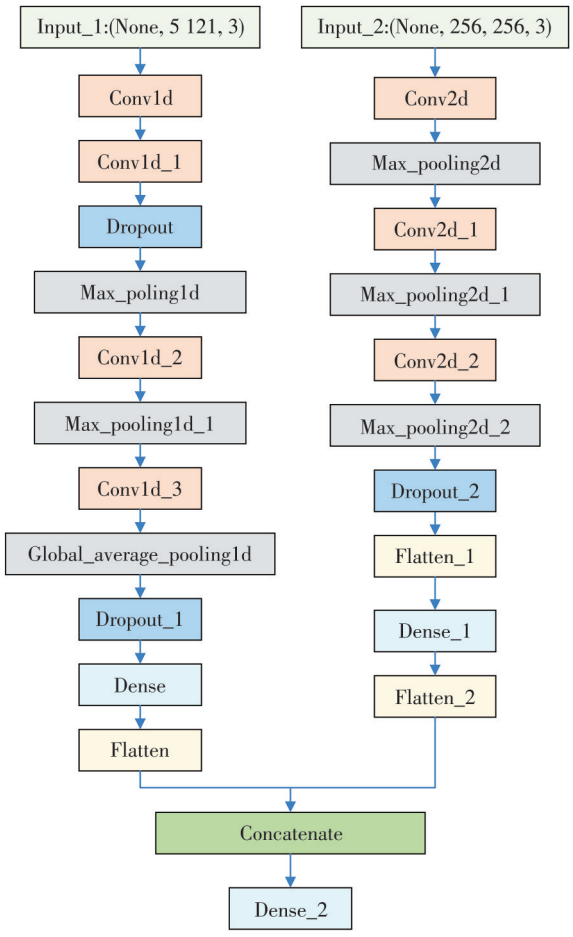

Fig. 2 Framework of VMD-CWT-CNN model

Since the proposed model is based on Keras framework, the Dense layer in Fig.2 represents the fully connected layer. The Input_1 layer and Input_2 layer represent the input layers of the one-dimensional path and the two-dimensional path, respectively (the shape of the training data in parentheses). The Conv layer represents the convolutional layer. The Max_pooling layer represents the Max Pooling layer. The Global_average_pooling layer represents the Global Average

Pooling layer. This model uses the SoftMax classifier, and the activation function uses the ReLU function.

The one-dimensional path of the model consists of 4 convolutional layers, 2 Max Pooling layers, 1 Global Average Pooling layer, 2 Dropout layers, 1 Dense layer and 1 Flatten layer. The two-dimensional path of the model consists of 3 convolutional layers, 3 Max Pooling layers, 1 Dropout layer, 1 Dense layer and 2 Flatten layers. First, the data pass through their respective path and are reorganized into a one-dimensional array in the Flatten layer. Then, the data are merged through the Concatenate operation. Finally, the classification results are output in Dense_2 layer.

3 Experimental design and data acquisition

The experimental platform consists of three parts: hydraulic system, electrical system and control system. The device diagram and schematic diagram are shown in Figs.3 and 4, respectively.

As shown in Fig.4, the power source of the experimental platform is composed of frequency converter 1 and asynchronous motor 2. The power output by asynchronous motor 2 directly acts on piston pump 6 (main pump) to drive it to rotate. The piston pump 6 (main pump), piston motor 14 (variable motor) and a series of components form a closed transmission system. Based on LabVIEW measurement and the control system, the variable frequency speed regulation of asynchronous motor 2 can be realized by changing the control voltage of frequency converter 1. The experimental platform uses a swash plate type axial piston pump and a swash plate type axial piston motor. The specific technical parameters are shown in Table 1.

Table 1 Variable pump/motor and main component parameters

Name	Model	Maximum displacement/ ($mL \cdot r^{-1}$)	Number of pistons
Variable pump	Linde HPV55-02RE1X300E	55	7
Variable motor	Linde HMV105-02E1C	105	9

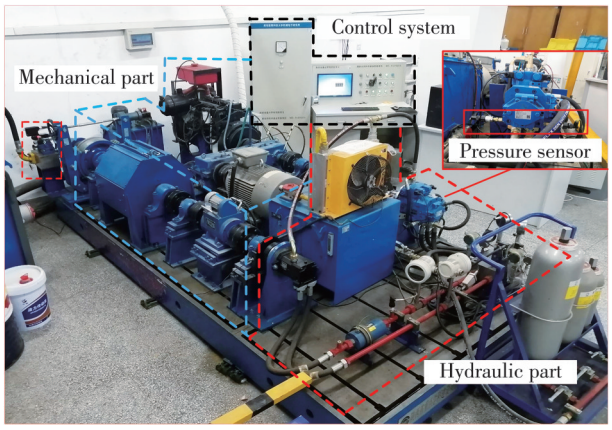

Fig. 3 Device diagram of experimental platform

Gear pump 16 and electromagnetic proportional relief valve 18 constitute the loading system of the experimental platform for digital simulation loading. By changing the opening of the orifice plate of proportional relief valve 18, the pressure of the load system and the load torque can be controlled.

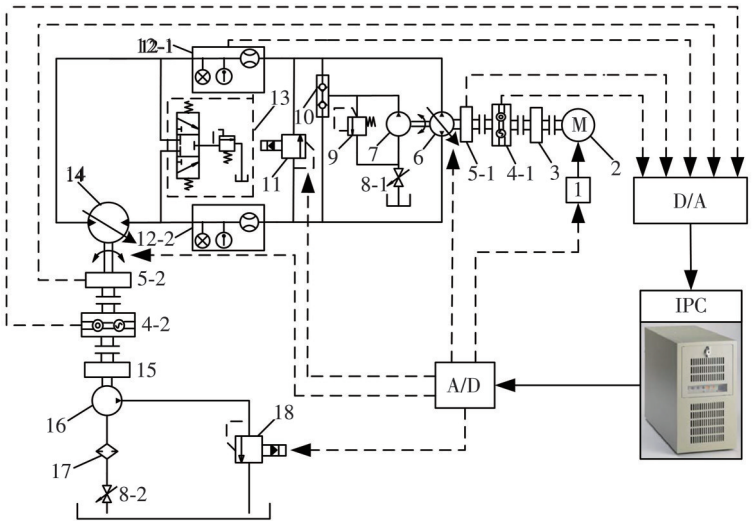

1—Inverter; 2—Asynchronous motor; 3—gearbox; 4-1, 4-2—Speed and torque sensors; 5-1, 5-2—Magnetoelectric speed sensors; 6—Main pump; 7—Oil filling pump; 8-1, 8-2—Electromagnetic relief valves; 9—Oil filling overflow valve; 10—Oil filling one-way valve; 11—Electromagnetic proportional overflow valve; 12-1, 12-2—Combined sensors; 13—Flush valve group; 14—Variable motor; 15—Inertia disk; 16—Gear pump; 17—Filter; 18—Electromagnetic overflow valve

Fig. 4 Schematic diagram of experimental platform

The vibration signal from the piston pump under different wear states of the valve plate was obtained by replacing the valve plate with different wear states into the piston pump under test. The valve plate in three wear

states is shown in Fig.5.

(a) Normal (b) Wear (c) Failure

Fig. 5 Valve plate states diagram

In the field measurement, 4 measurement points were selected as the position of the pump body close to the valve plate and X, Y, and Z directions of the pump body. After the vibration sensor was installed, the coco80 data acquisition instrument was used to acquire the signal of the vibration sensor, as shown in Fig.6. The performance parameters of vibration sensor are shown in Table 2.

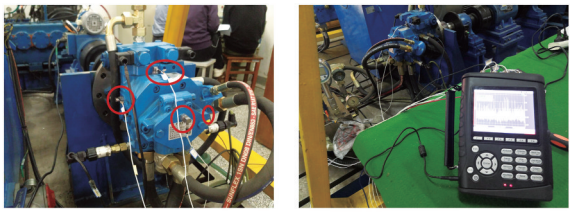

(a) Sensor layour diagram (b) Signal acquisition instrument

Fig. 6 Field measurement of vibration signal

Table 2 Vibration sensor parameters

Model	Sensitivity/(mV•g^{-1})	Frequency response/Hz	Range/g
Domestic IC type	100	0.5—5 000	4—20

We selected the sample data collected by the vibration sensor closer to the valve plate. When the experimental platform was in stable operation, the speed ranged from 300 r•m^{-1} to 1 400 r•m^{-1}, and 12 sets of data were recorded at an increase of 100 r•m^{-1} for each of the three wear states of valve plate.

4 Data partitioning and preprocessing

4.1 Data partitioning

The 12 sets of original data were collected, and 25 groups of small samples were obtained from each set. That is, there were 300 groups of small samples in each wear state. The experimental data samples were divided into 3 types according to the wear states (normal, wear, failure), 300 groups for each type, and a total of 900 groups. By labeling these 900 groups of small samples, mixing them up and dividing them into the training set and the validation set at a ratio of 7 ∶ 3, we obtained 630 groups of small samples in the training set, 270 groups of small samples in the validation set, as shown in Table 3.

Table 3 Experimental data division results

S/N (Label)	Wear states	Sample size/group	Total sample/group	Training set/group	Validation set/group
1	Normal	300			
2	Wear	300	900	630	270
3	Failure	300			

The experimental data acquisition and division process is shown in Fig.7.

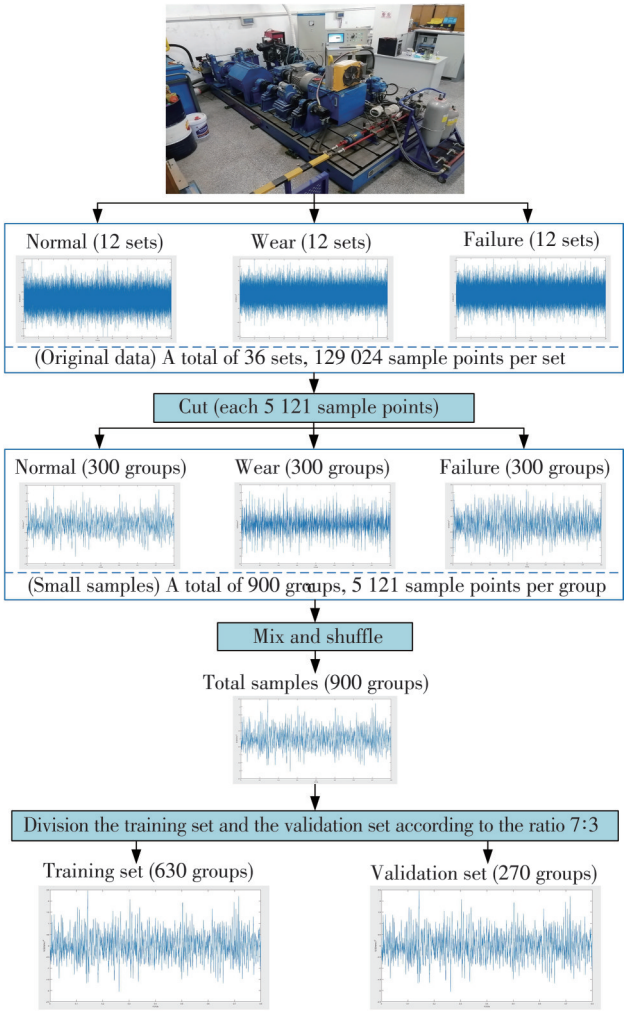

Fig. 7 Data acquisition and division process

4.2 Data preprocessing

Using the method described above, the number of VMD algorithm components, K, was determined based on the correlation coefficient between the components. Then, three IMF components were selected based on the maximum correlation coefficient and kurtosis and then recombined into a three-channel one-dimensional signal to send to the model. Normal signals of a group of piston pumps were randomly selected and decomposed by VMD. When the value of K is different, the corresponding maximum correlation coefficient is different, as shown in Table 4.

Table 4 Maximum correlation coefficient under different *K* values

K	Y_{max}
3	0.038
4	0.051
5	0.056
6	0.121

When K is 3, some information may be missed, so the value of K starts from 3, and the threshold is 0.1. It can be seen from Table 4 that when K is 6, the maximum correlation coefficient between the components after the signal is decomposed by VMD is greater than the threshold. When K is set at 3, 4 and 5, respectively, the maximum correlation coefficient is the largest when K is 5. The VMD effect is shown in Fig.8.

The optimized parameter is $K=5$, which means there are five IMF components. In the three wear states of valve plate, each state selects a set of data for VMD, and the correlation coefficient and kurtosis of each component are calculated, as shown in Table 5.

Table 5 Component parameters after VMD

State	Component	IMF1	IMF2	IMF3	IMF4	IMF5
Normal	Y	0.864	0.483	0.280	0.176	0.115
	Kurtosis	3.271	4.542	4.924	3.125	3.777
Wear	Y	0.480	0.370	0.373	0.557	0.439
	Kurtosis	2.776	3.081	3.143	4.184	5.295
Failure	Y	0.689	0.517	0.358	0.270	0.262
	Kurtosis	2.539	3.240	2.687	3.575	4.430

It can be seen from Table 5 that in the normal state, IMF1, IMF2 and IMF3 are the effective components; in the wear state, IMF2, IMF4 and IMF5 are the effective components; and in the failure state, IMF2, IMF4 and IMF5 are the effective components. In consideration of comprehensive effect, we selected IMF2, IMF4 and IMF5 as the effective components.

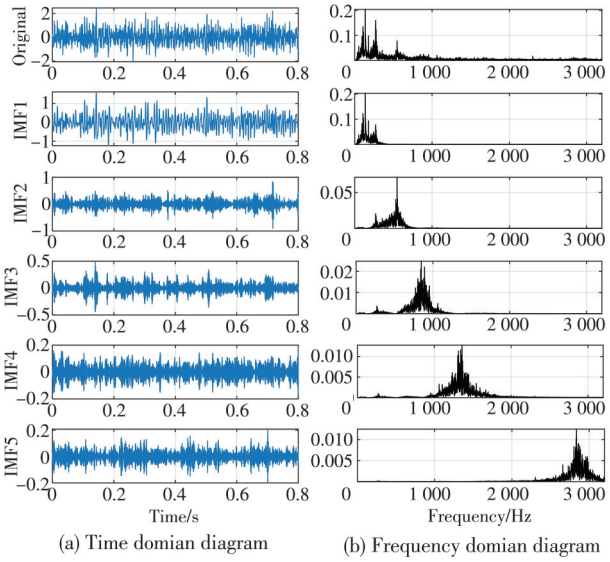

Fig. 8 VMD effect

After recombining the three components, the three-channel one-dimensional signal with a size of 5 121×3 pixels was obtained. After processing, part of the three-channel one-dimensional signals in the three wear states are shown in Fig.9.

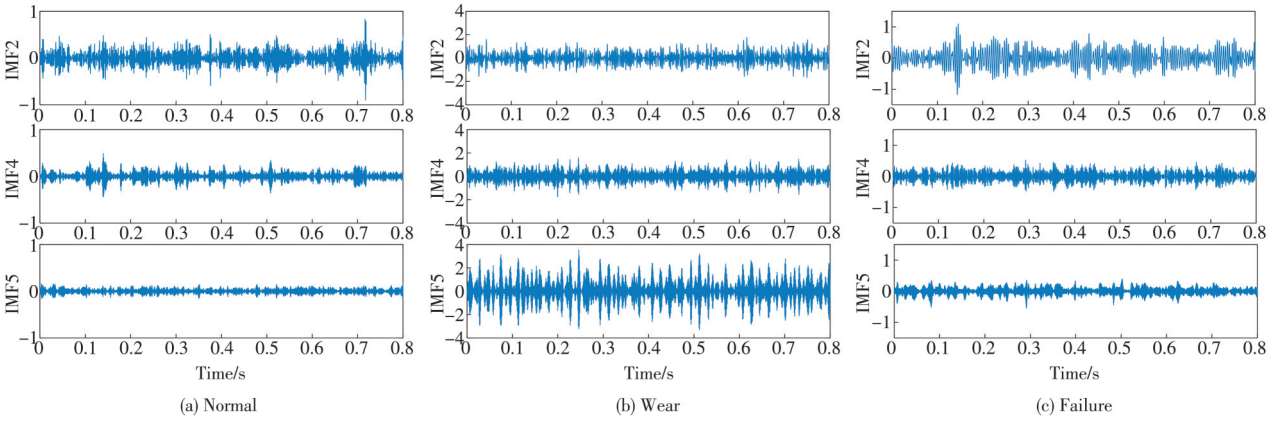

Fig. 9 Three-channel one-dimensional signals

The two-dimensional time-frequency diagram was obtained from the signal sets processed by CWT. Here, CWT was used to preprocess the sorted sample set, and then the two-dimensional wavelet time-frequency image with a size of 256×256×3 pixels was obtained as the image sample. The part of time-frequency diagrams of the three wear states are shown in Fig.10.

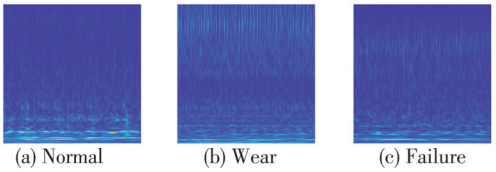

Fig. 10 Two-dimensional time-frequency diagrams of three wear states

Both VMD and CWT were realized by Matlab software.

5 Experimental results and analysis

5.1 Experimental process and results

The diagnostic flow chart of the wear states of the valve plate of the axial piston pump is shown in Fig.11.

Experimental process is as follows. Firstly, the original signal is obtained by the experimental platform and then divided cut into small sample groups. After being mixed and shuffled, these small sample groups are divided into the training set and the validation set at 7:3. Secondly, the samples were preprocessed. Three effective IMFs are obtained by optimized VMD and recombined into a three-channel one-dimensional signal. In addition, the two-dimensional time-frequency diagrams are directly obtained by CWT. Finally, these two types of signals are sent to the model for training, and the classification results are obtained.

The hardware configuration is as follows, CPU is intel CORE i5 9th, GPU is NVIDIA GTX1650, and the running memory has 16G. Python is used to build the CNN model in the TensorFlow + Keras environment.

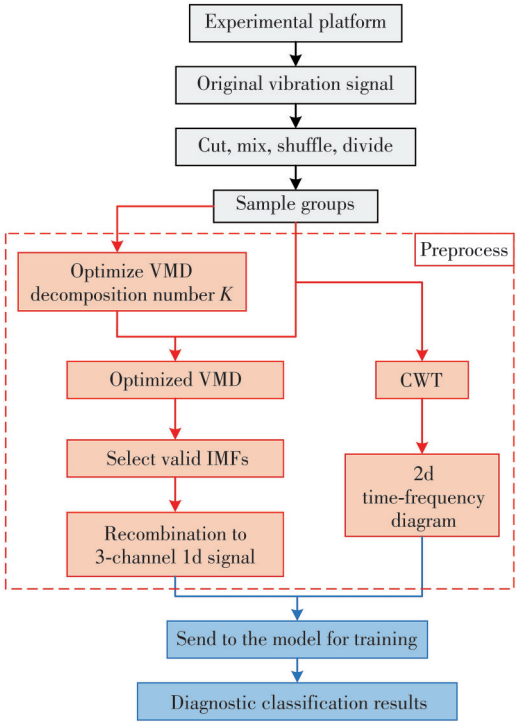

Fig. 11 Diagnostic flow chart of wear states of valve plate of axial piston pump

The performance of the samples in the process of passing through their own paths after inputting the samples into the model for training is shown in Fig.12.

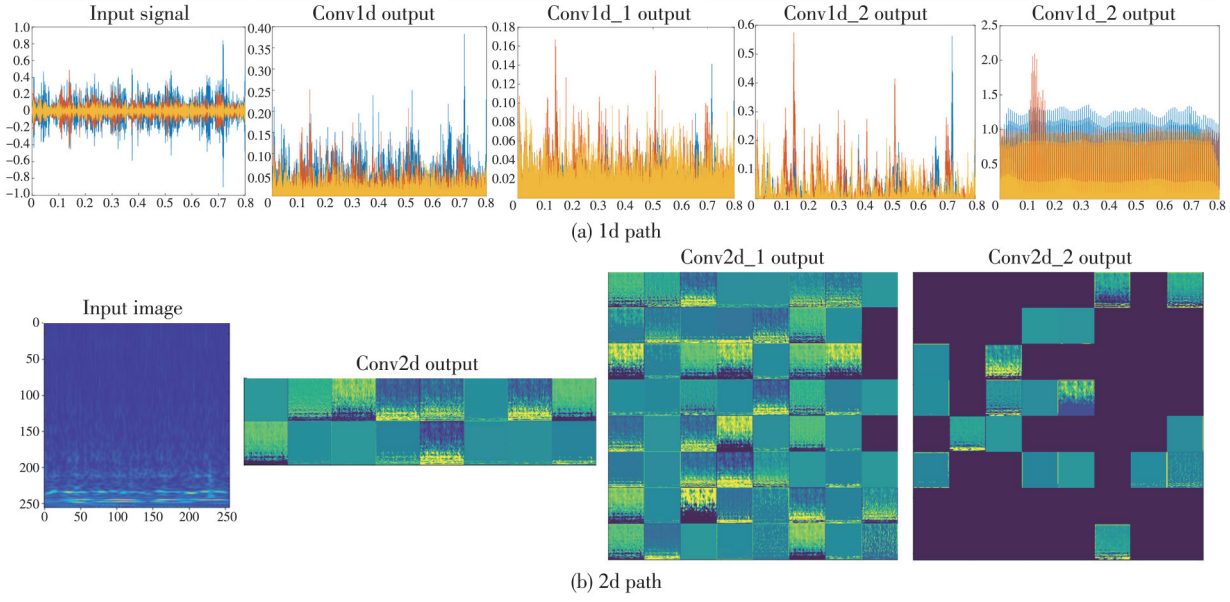

Fig. 12 Layer output of proposed model

It can be seen from Fig. 12 that the shallow convolutional layer is more sensitive to edges and prominent features. The deeper the convolutional layer, the more sensitive to subtle differences that are difficult to distinguish the convolutional layer.

The *t*-distribution stochastic neighbor embedding (*t*-SNE) is a visual analysis method for dimensionality reduction of high dimensional data. Its basic idea is to construct a *t*-distribution in low-dimensional space to make it consistent with the probability distribution in high-dimensional space. By using *t*-SNE, the layer output of the model were visualized, and the scatter plot of classification effect is shown in Fig.13.

It can be seen from Fig.13 that the distribution of the input layer is chaotic. After the shallow convolutional layer makes a preliminary distinction on the input, the degree of dispersion of the shallow convolutional layer is significantly greater than that of the input layer. With the continuous

deepening of the convolutional layer, the degree of dispersion becomes more and more obvious, and the fully connected layer of the respective path has a relatively good classification effect already. After merging the two paths, the combined fully connected layer has a very obvious distinguishing effect on the input samples.

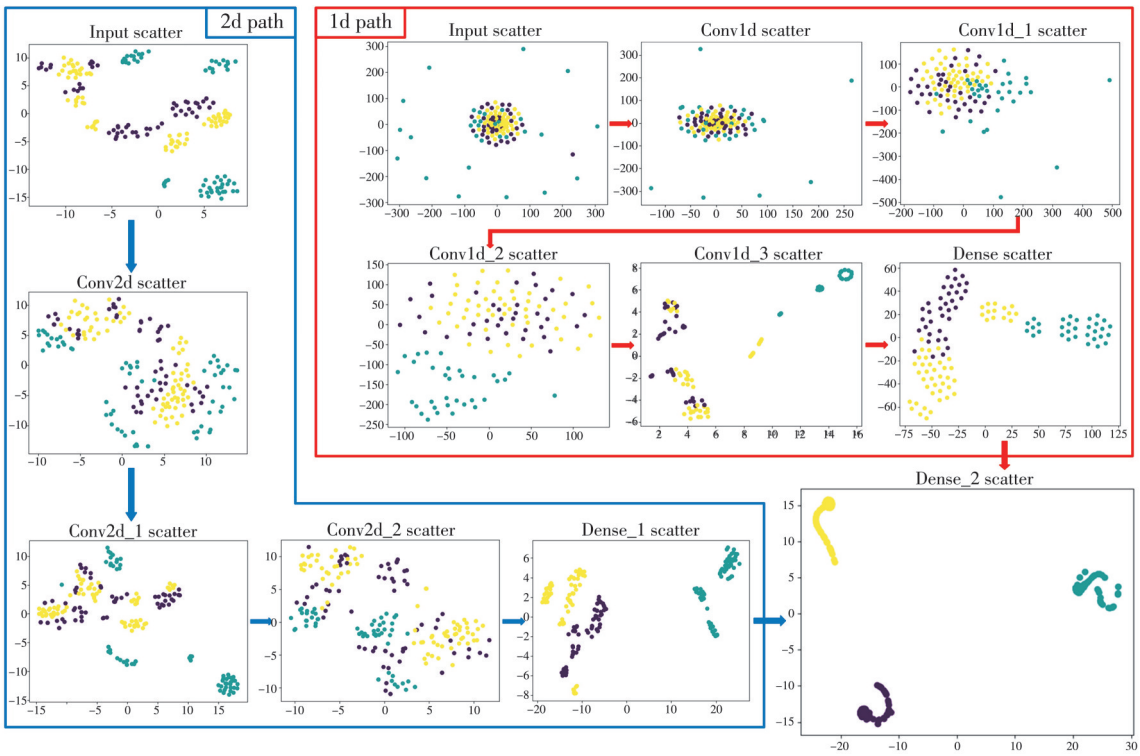

Fig. 13 Scatter plot of classification effect

The training accuracy and loss rate of the training set and the validation set of the model are shown in Fig.14.

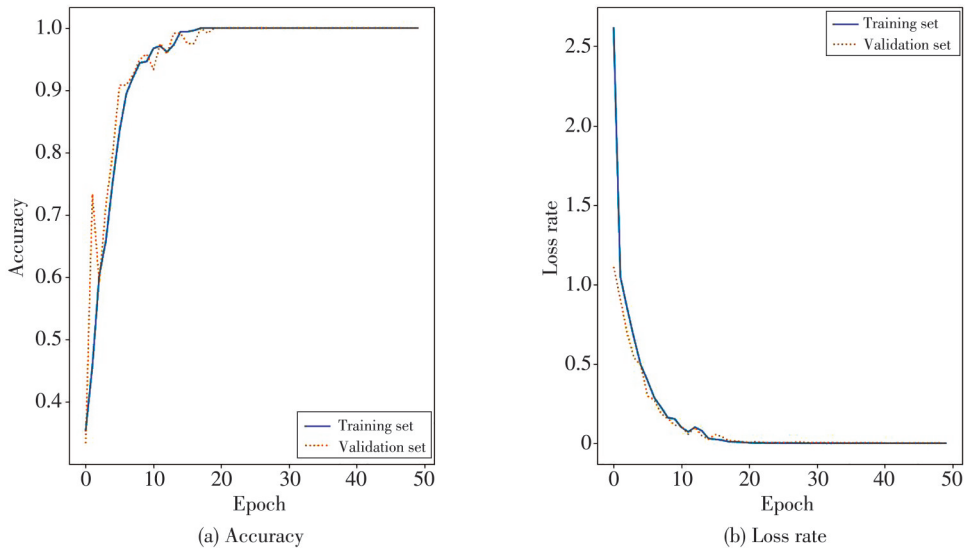

Fig. 14 Training results

As shown in Fig. 14. (a), the training curve of the validation set experiences a "steep rise" during the third iteration. This is because the parameters are continuously adjusted according to the training effect of the samples during the training process. In the early stage of training, due to the small amount of training and the uncertainty of the samples, there may be samples in the validation set that are more similar to the feature information in the training set. At this time, a neural network with parameters adjusted according to part of the training set is used to test the verification set, and the results produce a "steep rise". As the amount of training continues to increase, the training curve of the validation set tends to be stabilized, and the phenomenon of "steep rise" will not occur.

The iteration times of the model was set to be 50, and the batch size was set to be 40. Since there were 720 groups in the training set, the model was trained 18 times in each iteration. The model after training and

saving parameters was used to diagnose and classify the validation set. The confusion matrix of the classification result is shown in Fig.15. It can be seen that the optimal classification effect can actually be achieved via 25 iterations and reaches 99.7 %.

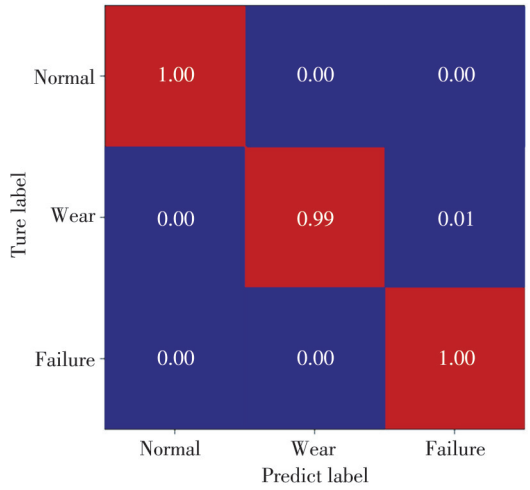

Fig. 15 Confusion matrix of classification effect

5.2 Comparative analysis

To verify the effectiveness of the proposed method. The optimized VMD-CWT-CNN model was split into two single-input CNN models: CWT-CNN model and optimized VMD-CNN model. The same data were sent to the three models for training with the same iterations. The classification accuracy is shown in Table 6.

Table 6 Comparison of classification accuracy values of three models

Model	Iterations/epoch	Accuracy/%
Optimized VMD-CNN	25	96.8
CWT-CNN	25	98.5
Optimized VMD-CWT-CNN	25	99.7

To further verify the effectiveness of the proposed method, the optimized VMD-CWT-CNN model was compared with BP neural network, multi-layer perceptron (MLP) and manual feature extraction+support vector machine classifier (FFT-SVM) model[18]. The BP neural network, the MLP and the optimized CWT-VMD-CNN model are implemented using Keras library with TensorFlow as the backend while the FFT-SVM model uses Scikit-learn library. The same data were sent to the three models for training with same iterations. The comparison of the classification accuracy is shown in Table 7.

It can be seen from Tables 6 and 7 that the training effect of the optimized VMD-CWT-CNN model is significantly better than that of the single-input model and other classic models.

Table 7 Comparison of classification accuracy of four classic models

Model	Iterations/epoch	Accuracy/%
BP	25	93.5
MLP	25	97.3
FFT-SVM	25	97.9
Optimized VMD-CWT-CNN	25	99.7

6 Conclusions

Aiming at the wear characteristics of the valve plate of the piston pump that are easily submerged by noise and difficult to extract, we proposed an intelligent state recognition method based on optimized VMD-CWT-CNN. The vibration signal was transformed into the two-dimensional time-frequency diagram with obvious characteristics, with the three-channel one-dimensional signal composed of IMFs as two types of the input of CNN. During the training of the model, the features were extracted from the respective paths and then fused in the fully connected layer. This method can achieve an accuracy of 99.7% in recognizing the wear states of the valve plate. Compared with other well-known neural networks and classic classifiers, the optimized VMD-CWT-CNN model showed better feature learning and classification performance, which proved the feasibility of this method. The optimized VMD-CWT-CNN provides a new idea for state recognition and failure diagnosis, and has a good prospect for technical application.

Acknowledgement

This work was supported by National Natural Science Foundation of China (No.51675399).

Declaration of conflicting interests

The authors have no conflict of interests related to this publication.

References

[1] LIU S, DING L, JIANG W. Study on application of Principal Component Analysis to fault detection in hydraulic pump//2011 International Conference on Fluid Power and Mechatronics, August 17-20, 2011, Beijing, China. Beijing: Acta Aeronautica et Astronautica Sinica, 2011: 173-178

[2] GU L, XU R, WANG N. A novel reduced order dynamic model of axial piston motors with compression flow losses and Coulomb friction losses. Industrial Lubrication and Tribology, 2020, 72(5): 567-573.

[3] ZI H Y. Application of the EEMD method to rotor fault diagnosis of rotating machinery. Mechanical Systems and

Signal Processing, 2009, 23(4): 1327-1338.
[4] JAYASWALT P, WADHWANI A K. Application of artificial neural networks, fuzzy logic and wavelet transform in fault diagnosis via vibration signal analysis: A review. Australian Journal of Mechanical Engineering, 2009, 7(2): 157-172.
[5] TANG X, LIANG L, GAO H, et al. Fault feature extraction method combining continuous wavelet transform with multi-constraint nonnegative matrix factorization. Journal of Vibration and Shock, 2013, 32(19): 7-11.
[6] HONG L, WANG W, CHEN Q. State identification of draft tube vortex based on continuous wavelet transform and convolution neural network. Guangdong Electric Power, 2018, 31(5): 1-6.
[7] WU S, FENG F, WU C, et al. Research on fault diagnosis method of tank planetary gearbox based on VMD-DE. Journal of Vibration and Shock, 2020, 39(10): 176-185.
[8] ZHOU F, TANG J, HE Y. Unbalanced fault feature extraction for wind power gearbox based on improved VMD. Journal of Vibration and Shock, 2020, 39(5): 170-176.
[9] FENG S, CHAI K, ZHU S, et al. Fault feature extraction of hydraulic system based on improved VMD. Journal of Naval University of Engineering, 2021, 33(2): 6-13.
[10] ZHENG Y, BAO H, XU C. A method for improved pedestrian gesture recognition in self-driving cars. Australian Journal of Mechanical Engineering, 2018, 16(sup1): 78-85.
[11] ZHANG W, LI C, PENG G, et al. A deep convolutional neural network with new training methods for bearing fault diagnosis under noisy environment and different working load. Mechanical Systems and Signal Processing, 2018, 100: 439-453.
[12] WU C, JIANG P, DING C, et al. Intelligent fault diagnosis of rotating machinery based on one-dimensional convolutional neural network. Computers in Industry, 2019, 108: 53-61.
[13] MONTEIRO R, BASTOS-FILHO C, CERRADA M, et al. Convolutional neural networks using fourier transform spectrogram to classify the severity of gear tooth breakage// International Conference on Sensing, Diagnostics, Prognostics, and Control, August 15-17, 2018, Xi′an, China. Piscataway, N. J.: IEEE, 2018: 490-496.
[14] SIMONYAN K, ZISSERMAN A. Two-stream convolutional networks for action recognition in videos. Advances in Neural Information Processing Systems. 2014-06-09[2022-05-09]. https://doi. org/10. 48550/arXiv. 1406. 2199.
[15] DONG H, KONG C, SHI F, et al. Signal processing of ultrasonic phased array echo of borehole imaging testing. Nondestructive Testing, 2017, 39(5): 65-69.
[16] DRAGOMIRETSKIY K, ZOSSO D. Variational mode decomposition. IEEE Transactions on Signal Processing, 2014, 62(3): 531-544.
[17] YANG S, GU L, SHI Y, et al. Monitoring method of gear teeth failure of hydraulic gear pump based on improved VMD and DBN-DNN of electrical signal. Journal of Measurement Science and Instrumentation, 2021, 12(2): 242-252.
[18] BING L, JING C, XIAO J, et al. Robotic impact-echo non-destructive evaluation based on FFT and SVM// 11th World Congress on Intelligent Control and Automation, June 2-4, 2014, Shenyang, China. Piscataway, N. J.: IEEE, 2014: 2854-2859.

一种基于优化 VMD-CWT-CNN 的柱塞泵配流盘磨损状态识别方法

吕尚杰*, 谷立臣, 耿宝龙

西安建筑科技大学 机电工程学院, 陕西 西安 710055

摘　要：为解决一维振动信号难以充分挖掘表达状态特征信息以及柱塞泵配流盘磨损早期识别问题，基于卷积神经网络（Convolutional neural networks，CNN）优秀的图像处理能力，提出了一个优化 VMD-CWT-CNN 模型。首先，采用连续小波变换（Continuous wavelet transform，CWT）对信号进行预处理，得到信号的二维时频图，作为 CNN 模型的一路输入，将状态识别问题转化为 CNN 图像识别问题。 其次，基于相关系数对变分模态分解（Variational mode decomposition，VMD）参数优化后，利用优化 VMD 对振动信号进行预处理，再以相关系数和峭度值最大为优选原则，甄选出三组蕴含故障特征的本征模态函数（Intrinsic mode function，IMF），将其重组为三通道一维信号，作为 CNN 模型的另一路输入。最后，在 CNN 模型中将两路信息汇聚并得到柱塞泵配流盘磨损状态识别分类结果。实验中，此方法分别采用优化 VMD 和 CWT 对振动信号预处理，再结合 CNN 对磨损状态进行分类。实验结果表明，该方法对于配流盘磨损的三种状态的识别效果显著优于单路输入的 CNN 模型以及典型的深度学习方法和机器学习分类器。因此，优化的 VMD-CWT-CNN 方法可以更准确地实现柱塞泵配流盘磨损状态识别。

关键词：柱塞泵配流盘磨损；振动信号；卷积神经网络；变分模态分解；连续小波变换

引用格式：LYU Shangjie, GU Lichen, GENG Baolong. A recognition method of valve plate wear states of piston pump based on optimized VMD-CWT-CNN. Journal of Measurement Science and Instrumentation, 2024, 15(1): 43-53.